IEEE Access
Multidisciplinary ⋮ Rapid Review ⋮ Open Access Journal

Received December 1, 2021, accepted December 19, 2021, date of publication December 22, 2021,
date of current version January 12, 2022.

Digital Object Identifier 10.1109/ACCESS.2021.3137716

Orthogonal Chirp-Division Multiplexing for Future Converged Optical/Millimeter-Wave Radio Access Networks

COLM BROWNING[1], (Member, IEEE), DEVIKA DASS[1], (Student Member, IEEE), PAUL TOWNSEND[2], (Member, IEEE), AND XING OUYANG[2], (Member, IEEE)

[1]School of Electronic Engineering, Dublin City University, Glasnevin, Dublin 9, Ireland
[2]Photonic Systems Group, Tyndall National Institute, Cork, T12 R5CP Ireland

Corresponding author: Colm Browning (colm.browning@dcu.ie)

This work was supported by the Science Foundation Ireland under Grant 18/SIRG/5579 and Grant 12/RC/2276-P2.

ABSTRACT Envisaged network scaling in the beyond 5G and 6G era makes the optical transport of high bandwidth radio signals a critical aspect for future radio access networks (RANs), while the move toward wireless transmission in millimeter-wave (mm-wave) and terahertz (THz) environments is pushing a departure from the currently deployed orthogonal frequency division multiplexing (OFDM) modulation scheme. In this work, the orthogonal chirp-division multiplexing (OCDM) waveform is experimentally deployed in a converged optical/mm-wave transmission system comprising 10 km analog radio-over-fiber (A-RoF) transmission, remote mm-wave generation and 2 m wireless transmission at 60 GHz. System performance is evaluated in terms of both bit error ratio (BER) and error vector magnitude (EVM) for a wideband 4 GHz 16 Gb/s signal and 128/256-Quadrature Amplitude Modulation (QAM) mobile signals compatible with 5G new radio numerology. OCDM is shown to outperform OFDM by offering enhanced robustness to channel frequency selectivity, enabling performances below the forward error correction (FEC) limit in all cases and exhibiting an EVM as low as 3.4% in the case of the mobile signal transmission.

INDEX TERMS Chirp modulation, millimeter wave communication, optical fiber networks, radio access networks.

I. INTRODUCTION

The delivery of 5G mobile communications is well underway and is driving network evolution today. From the current standpoint it is difficult to say exactly what will constitute the 6G era of mobile communications but it is clear that, as well as the key drivers of increased bandwidth, lower latency and enhanced connectivity, future wireless communications must facilitate scaling in a way that supports a vast array of user types (human and otherwise) in potentially challenging environments [1], [2]. This points to the 'super-convergence' of emerging flexible radio and optical technologies and network types which are capable of providing a variety of extremely high-throughput services in diverse environments [2], [3]. 5G's frequency range 2 (FR2) has standardized the use of mm-wave frequencies up to 48 GHz in order to deliver enhanced mobile channel bandwidths of up to 400 MHz. This trend looks set to continue with higher frequency mm-wave ranges (around 60 GHz and 90 GHz) and THz frequencies (0.1 - 1 THz) being identified as key platforms for developing high bandwidth and multi-Gb/s wireless technologies for 'beyond' 5G and 6G [4]. Indeed, outside of current mobile standards, WiGig protocols, including the recently released 802.11ay standard [5], specify multi-GHz mm-wave channel bandwidths for the delivery of 10's Gb/s per channel in the 60 GHz unlicensed band.

The key optical infrastructures charged with the delivery of broadband and mobile services are the passive optical network (PON) and the RAN, respectively. A central unit (CU), distributed unit (DU) and remote unit (RU) constitute the three main functional elements of a RAN. Various RAN topologies can be implemented through the relative distribution of these elements along the path from the RAN's central office (CO) to the antenna site, and these are well summarized in [6]. A more centralized RAN (C-RAN) design, allowing the CU and DU functionalities to be co-located at the CO,

The associate editor coordinating the review of this manuscript and approving it for publication was Xihua Zou.

is preferable in cases where the footprint and cost of the antenna site are of primary concern. Considering the vast proliferation of antenna sites envisaged beyond 5G, and the antenna site complexity synonymous with the transmission of very high frequency carriers, it is likely that a highly centralized RAN architecture will be required to facilitate scaling for wireless networks incorporating THz and mm-wave functionality. Increased centralization of RAN resources at the CO emphasises the role of RoF transport of mobile data between the CO and the RU (i.e. fronthaul) which can span 10-20 km's. As the number of users and antenna sites grow, the associated increase in fronthaul capacity demands has shifted focus away from simplistic point-to-point fronthaul links, to those harnessing optical access networking technologies such as wavelength division multiplexing (WDM) [7], [8]. Unsurprisingly, these trends have led to proposals for the co-operation of PON and C-RAN infrastructures whereby RAN traffic can be provisioned over a PON topology — and indeed such operation is included in the ITU G-series recommendations [9].

The recent deployment of enhanced-common public radio interface (eCPRI) technology has provided some improvement in spectral efficiency for current fronthaul transmission, but this is ultimately limited by the binary modulation scheme currently employed. An alternative approach is to use Analog (i.e. multi-carrier) RoF (A-RoF), whereby the mobile signal is transmitted over the fronthaul link in its native multi-carrier format [10]. At the cost of decreased robustness to system nonlinearity, this technique provides excellent spectral efficiency and results in the simplification of the RU site compared to a D-RoF approach — ultimately facilitating network antenna 'densification'.

The authors' prior works have examined how remote mm-wave generation through optical means can be incorporated into a C-RAN architecture [11], [12]. This type of optical-wireless converged system design makes use of the optical heterodyne operation whereby two optical carriers, centrally distributed over a fronthaul link, undergo heterodyne detection at a photo-diode (PD) stage at the antenna site; producing a mm-wave signal for wireless propagation. This approach avoids the difficulty/expense of mm-wave carrier generation in the electronic domain, is capable of providing a wide mm-wave carrier tuning range and offers relative ease of convergence with the hardware centralized implementation of C-RAN. Optical heterodyning in this way can introduce significant amounts of optical phase noise and frequency offset which are performance limiting factors for A-RoF systems [11]. Our prior work has proposed several hardware and software based techniques to mitigate these effects [13], thereby alleviating strict optical source linewidth and stability requirements and making remote optical heterodyne operation a viable option for future mm-wave A-RoF fronthaul.

Nevertheless, other challenges associated with operation in the mm-wave and THz regime, such as frequency selective fading, severe multi-path interference and enhanced amplitude noise effects remain highly problematic. To tackle these, a departure from the 4G/5G waveform of choice — OFDM — is expected [2]. Recently, we demonstrated the use of the novel waveform orthogonal chirp division multiplexing (OCDM) in a converged optical / mm-wave system [14]; OCDM was shown to outperform equivalent OFDM signals in the system owing to its robustness to channel fading (assigned by its chirp spread-spectrum form [15], [16]) and its capability of providing enhanced channel estimation. The authors of [17] have previously demonstrated the application of OCDM in a RAN implementation incorporating optical heterodyne operation and mm-wave wireless transmission — with results aimed at highlighting OCDM's tolerance to interference from adjacent wireless services. In this work, we augment our previous OCDM converged system analysis by demonstrating an end-to-end C-RAN transmission path including 10 km A-RoF fronthaul and 2 m wireless transmission at 60 GHz. In addition to performance evaluation using equivalent 5G new radio (NR) OCDM/OFDM compatible signals with up to 256-QAM, a 4 GHz bandwidth OCDM signal delivering 16 Gb/s is successfully transmitted over the link, exhibiting near-uniform performance across the frequency range; highlighting OCDM's potential to provide extremely high throughput future mm-wave wireless communications enabled through converged optical networking.

II. MILLIMETER-WAVE ENABLED OPTICAL RADIO ACCESS NETWORKS

As the developments in radio access domain are leading to an increased reliance on optical transport and the deployment of mm-wave mobile communications, it is not surprising that much research of late has investigated various options for C-RAN designs incorporating optical fronthaul and mm-wave functionality. Table 1 summarizes the key details and metrics of some state-of-the-art mm-wave enabled C-RAN demonstrations. These demonstrations — all of which include optical fronthauling — can be broadly broken into two categories; (i) those which use electronic methods for up-conversion to mm-wave frequencies and (ii) those which use photonic methods for mm-wave generation (i.e. optical heterodyning). In the case of the former, the requirements on the optical source are reduced as simple intensity modulation/direct detection (IM/DD) schemes (using low cost commercial directly or externally modulated lasers DML/EML, for example) can be used to transmit baseband or intermediate frequency (IF) modulated data over the fronthaul link. This relative simplicity of the optical transceiver design comes at the expense of increased electronic complexity as high frequency local oscillators (LOs) are required to up-convert the information signal to the target mm-wave band at the RU [19], [20]. In [21], the data signal is up-converted to a mm-wave frequency before being modulated onto the optical carrier at the CO. This reduces the complexity of the RU but requires a modulator with sufficient (mm-wave) bandwidth at the CO.

The second category of demonstrations incorporates photonic generation of mm-wave signals into the C-RAN design.

TABLE 1. State-of-the-art millimeter-wave enabled C-RAN demonstrations.

Ref.	mm-wave Generation	Optical Source	Frequency (GHz)	UL/DL	Fronthaul (km)	RoF Modulation	Wireless Transmission	Data Rate (Gb/s)
[18]	N/A	Fiber Laser + MZM	38/26.5	UL	20	OFDM/QAM	No	0.5 (MC) 60 (SC)
[19]	Elec. Up-Conv. @ RU	DML	28	UL&DL	1	OFDM (Multi-band)	Yes (4×4 MIMO)	9 (real time)
[20]	Elec. Up-Conv. @ RU	DFB/EML	60	UL&DL	7	QAM/QPSK (Multi-band)	Yes	24
[21]	Elec. Up-Conv. @ CO	DFB	33	DL	15	OFDM w/ BPSK	Yes	4 (MC) 10 (SC)
[22]	Opt. Heterodyne (Cars. @ CO/RU)	ECL×2	61	DL	10	QAM (Coherent)	No	64
[23]	Opt. Heterodyne (Carriers @ CO)	Dual Fiber Laser	65.12	DL	20	OFDM	Yes	20
[24]	Opt. Heterodyne (Carriers @ CO)	ECL + MZM	28	DL	10	OFDM (Multi-band)	Yes	4.8
[25]	Opt. Heterodyne (Carriers @ CO)	'CW' + SiP MZM	40	DL	20	OFDM	No	7.8
[26]	Opt. Heterodyne (Carriers @ CO)	DFB + MZM	60.25	DL	3	QAM (NOMA encoding)	Yes (Multi-Access)	8
[27]	Opt. Heterodyne (Carriers @ CO)	MLL	60	DL	25	OFDM	No	1.17
[17]	Opt. Heterodyne (Carriers @ CO)	DFB + Phase Mod.	57.2	DL	15	OCDM/OFDM	Yes	5.33
This Work	Opt. Heterodyne (Carriers @ CO)	DFB (Optical Frequency Comb)	60.5	DL	10	OCDM/OFDM	Yes	16

UL: Uplink, **DL**: Downlink, **MC**: Multi-Carrier, **SC**: Single-Carrier, **DML**: Directly Modulated Laser, **DFB**: Distributed Feedback Laser, **EML**: Externally Modulated Laser, **BPSK**: Binary Phase Shift Keying, **ECL**: External Cavity Laser, **CW**: Continuous Wave, **SiP**: Silicon Photonic, **NOMA**: Non-Orthogonal Multiple Access, **MLL**: Mode Locked Laser

This has the impact of significantly altering the requirements of the optical sources used, as Table 1 highlights. Recent demonstrations [22], [23] achieving high data rate transmission make use two discrete low noise lasers, adding considerably to source complexity and expense. Other demonstrations [17], [24]–[26] listed deploy a single optical source followed by a modulator which is driven such that two correlated optical tones are produced. This is a common approach that can facilitate the use of low cost commercial lasers but incurs the insertion loss and added bulk associated with the requirement for an additional (null-biased) modulator at the CO. A mode locked laser (MLL) is used in [27] to provide carriers for heterodyne operation, requiring optical feedback for carrier linewidth reduction. The system design presented in this work aims to take advantage of the flexibility and reduced RU complexity offered by the optical heterodyne approach while also employing a low-cost and small footprint solution for coherent carrier generation at the CO though the use of an optical frequency comb generated by gain-switching a commercial DFB laser [11].

Overall, it is likely that the relative trade-offs between RF and optical complexity associated with mm-wave C-RAN designs will be evaluated in the context of the mm-wave frequency range required for a specific network type or application. For near-term systems targeting lower mm-wave frequencies ∼28 GHz, electronic up/down-conversion may be a more attractive option, helping to maintain compatibility with today's optical access infrastructure. As future mm-wave communications move to ranges around 60 and 90 GHz, the ability to provide high bandwidth and flexible mm-wave generation at these frequencies, in tandem with the potential for RU simplification, greatly strengthens the case for the deployment of optical heterodyne based fronthaul systems.

III. ORTHOGONAL CHIRP-DIVISION MULTIPLEXING

A. WAVEFORM

Much research is currently underway examining waveform design in wireless systems for the beyond 5G and 6G era. Considering the diversity in transmission paths and applications required, it is likely that several application specific modulation formats will be deployed. One such candidate is OCDM which was previously proposed by the co-authors [15]. In the near term, the use of mature OFDM technologies will be sustained through the deployment of 5G systems. With OFDM, at the transmitter side, the data to be transmitted (typically in QAM format) is parallelized and used as an input to an inverse discrete Fourier transform (IDFT). Each parallel input modulates one of a finite set of orthogonal frequency subcarriers assigned by the IDFT. The orthogonal components are summed and then serialized to form an output OFDM symbol which contains all subcarriers

spaced in the frequency domain by a value equal to the OFDM symbol rate.

Conceptually, OCDM generation is very similar. Here, instead of an IDFT, an inverse discrete Frensnel transform (IDFnT) is used to provide a set of orthogonal chirps which are modulated with the input parallel (QAM) data — see further details in [15]. By switching to this chirp-based approach, each of the parallel QAM data inputs are modulated across a range of frequencies rather than being localized in frequency on a single subcarrier, as is the case with OFDM. This spread-spectrum feature of the OCDM signal increases the signal's robustness to frequency selectivity in the channel. Unlike other spread-spectrum techniques, OCDM's multi-carrier form (assigned through the Fresnel transform) allows it to maintain the same spectral efficiency as the equivalent OFDM signal. Furthermore, OCDM's (I)DFnT can be synthesized utilizing the (I)DFT as a basis; offering ease of integration with existing OFDM digital signal processing (DSP).

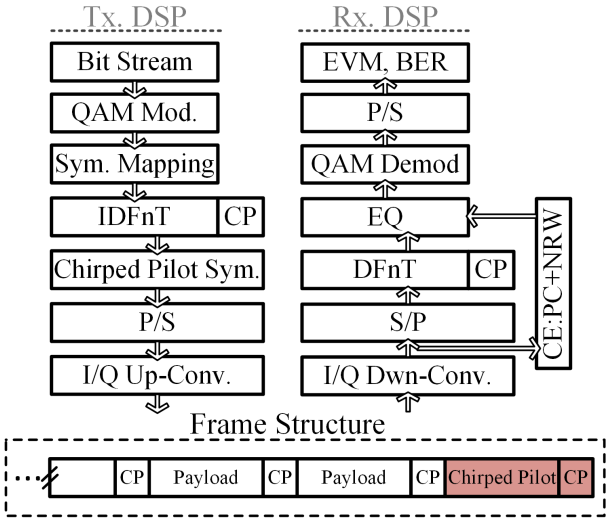

FIGURE 1. Transmitter and receiver side DSP associated with intermediate frequency OCDM generation/reception and the time domain signal frame structure.

B. CHANNEL ESTIMATION AND DSP

Another advantage of OCDM is its inherent compatibility with pulse compression (PC) based channel estimation (CE) — a well known CE technique in radar systems. Considering that a transmitted OCDM signal consists of a set of frequency chirps, it follows that it is possible to estimate the channel frequency response (CFR) by analyzing a received chirped signal which contains channel state information (CSI) across the entire OCDM signal bandwidth. Practically, this means that a single chirp component obtained directly from OCDM's DFnT can be used as a pilot signal enabling PC CE at the receiver. In order to improve the accuracy of this CE, a noise rejection window (NRW) is proposed in [28] to remove excess noise after PC. The resultant estimator is shown to be unbiased and to converge on the actual channel CSI, unlike frequency-domain averaging methods typically employed with OFDM. Further details of this process can be found in [28] which demonstrates that the PC+NRW CE provides the same performance as a minimum mean squared error (MMSE) estimator with reduced computational complexity, and requires one additional DFnT (in addition to the NRW function) compared to standard single-tap frequency domain equalization process.

Fig. 1 shows a block diagram of the DSP processes used to generate and receive multi-carrier OCDM signals as well as the frame structure of the transmitted OCDM signal. The diagram represents a very similar sequential routine to that associated with OFDM, with the replacement of the traditional (I)DFT blocks with IDFnT blocks and the addition of a chirped pilot signal (enabling receiver CE using PC in conjunction with NRW). The In-phase (I) and Quadrature (Q) mixing stages shown at the end of the transmitter side and start of the receiver side are implemented for digital IF up/down conversion — although these process could easily be implemented in the analog domain.

IV. EXPERIMENTAL SETUP

The experimental optical/mm-wave transmission system setup is shown in Fig. 2. A gain-switched optical frequency comb (GSOFC) is used to provide multiple correlated optical carriers each with a spacing of 18.7 GHz (see output optical spectra in Fig. 4(a)). This GSOFC is generated by using an 18.7 GHz sinusoid — which emanates from an RF synthesizer and is amplified to +17 dBm — to directly modulate a 20 GHz bandwidth commercial DFB from NEL which is biased at 62 mA. From the resulting OFC, a wavelength selective switch (WSS) is used to filter two carriers which have a frequency spacing of 56.1 GHz between them. Both carriers are then amplified with an Alnair low noise Erbium doped fiber amplifier (EDFA) to +18 dBm to overcome losses introduced by the transmitter filtering and modulation stages. Following amplification, a 50:50 splitter directs the light to two parallel arms. The lower arm contains a polymer-based I/Q modulator from GigOptix and a free-space Yenista tunable optical bandpass filter (TOBPF). The I/Q modulator is used along with an electrical 90° hybrid to perform single sideband (SSB) modulation of the optical carrier with the driving electrical IF (4.4 GHz) OFDM/OCDM signals (details below) which are output from a Tektronix 70002A arbitrary waveform generator (AWG) operating at 20 GSa/s. The TOBPF is used to isolate the carrier and data sideband, rejecting unwanted spectral components including the residual suppressed sideband. The upper arm contains a variable optical delay line and another Yenista TOBPF. The delay line is used to compensate the mismatch in effective path lengths experienced by both the modulated and un-modulated optical carriers in the transmission system. A delay of 200 ps is set throughout the work to compensate for this mismatch which arises primarily from the differing patch cords and components used in both arms of the transmitter, but is also contributed to by the effects of fiber dispersion

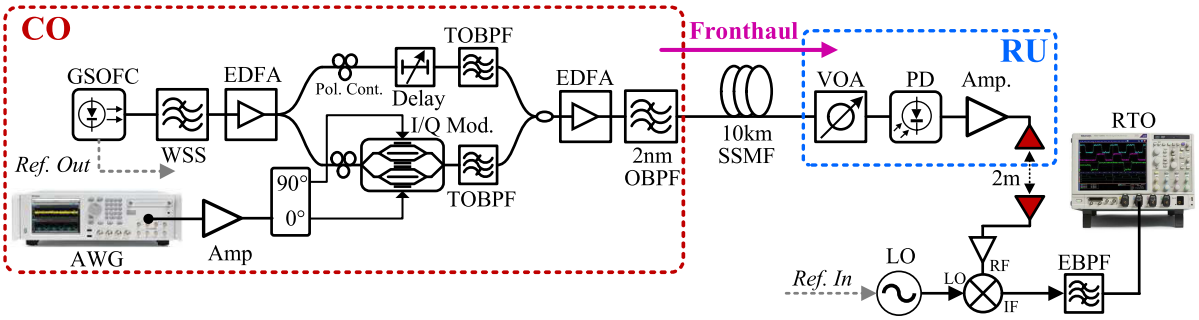

FIGURE 2. Experimental optical/mm-wave system setup incorporating a 10 km optical fronthaul link and 2 m wireless transmission. The dashed lines indicate the proposed placement of equipment within the context of a centralized RAN.

during transmission. The path patching procedure enables carrier coherence to be maintained at the receiver PD stage and hence minimizes the mm-wave carrier phase noise produced through the optical heterodyne process [11]. A 50:50 coupler combines the two arms before the composite signal (see optical spectrum Fig. 4(b)) is amplified using an Amonics EDFA to a launch power of +5 dBm. The various CO architecture and components used are highlighted in red in the photograph of the experimental setup in Fig. 3(a). The signal is then transmitted over 10 km of standard single mode fiber (SSMF). At the optical receiver a variable optical attenuator (VOA) is used to control the power falling on a 70 GHz bandwidth PIN PD. Following photo-mixing at the PD, the produced mm-wave data signal at 60.5 GHz (56.1 GHz + 4.4 GHz) is amplified using a 55 - 65 GHz electrical amplifier and is then transmitted over a 2 m point-to-point wireless link using a pair of 20 dB gain 55 - 65 GHz directional horn antennae (see the wireless link and RU components in the laboratory setup pictures in Figs. 3(a) and (b), respectively). The received mm-wave signal is amplified and then mixed with a 56.1 GHz LO — which is phase locked to the transmitter through a reference signal from the RF synthesizer used to generate the OFC — using a mm-wave mixer. The output IF signal passes through an electrical bandpass filter (EBPF) before being captured using a Tektronix MSO 71254C real time oscilloscope (RTS) operating at 50 GSa/s (see the mm-wave receiver setup photograph in Fig. 3(c)). The sampled IF signal is then processed offline using the Rx. DSP blocks outlined in Fig. 1.

For performance comparisons, equivalent OFDM and OCDM signals are evaluated in the transmission system. OCDM signals are generated offline using the Tx. DSP blocks shown in Fig. 1. OFDM signals are generated in a similar fashion with the (I)DFnT blocks in Fig. 1 replaced with standard (I)DFT blocks. While PC+NRW channel estimation is enabled by the insertion of a chirped pilot symbol inherent to OCDM, OFDM signals at the transmitter are generated both with and without an appended chirped pilot symbol. This allows OFDM performance to be evaluated in cases where PC+NRW CE and standard frequency domain estimation (FDE) are used. For both OFDM and OCDM,

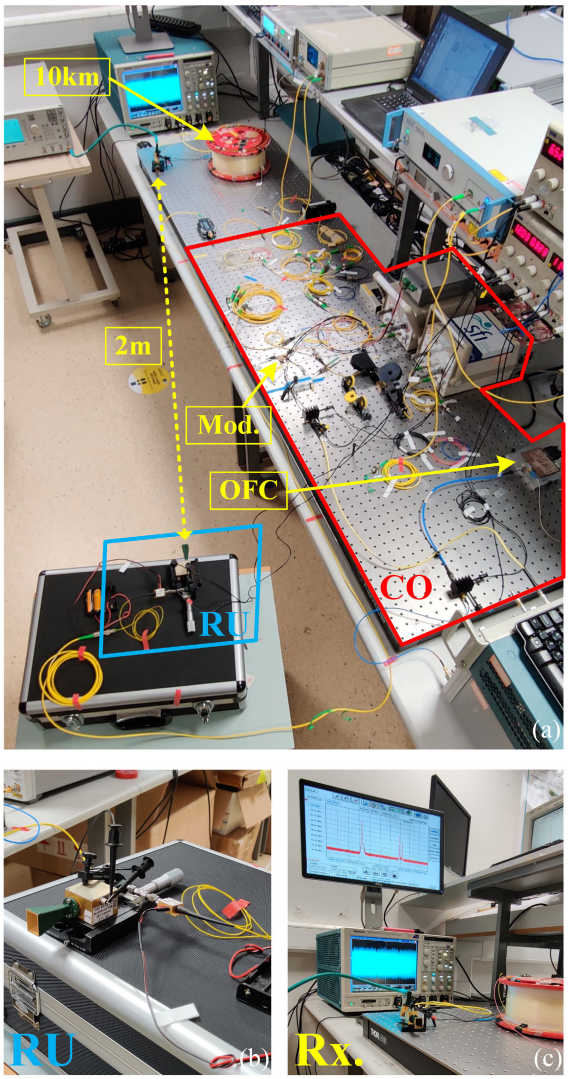

FIGURE 3. Photographs of (a) the complete hybrid optical/mm-wave laboratory set-up at Dublin City University and close ups of (b) the RU components and (c) the mm-wave receiver components.

the chirped pilot symbol is added to the beginning of each generated sequence as shown by the signal frame structure in Fig. 1 (further details of pilot symbol generation can be

TABLE 2. Wideband and 5G signal numerologies.

Prop.	Wideband	Mobile (5G)	Unit
# Chirps/SCs	128	820	n/a
(I)DF(n)T size	256	1024	n/a
QAM order	16	128 / 256	n/a
Symbol Rate	311.25	0.244	MHz
Bandwidth	4000	200.2	MHz
Cyclic Prefix	6.25	6.25	%
Raw Data Rate	16	1.4 / 1.6	Gb/s

SC: Subcarrier

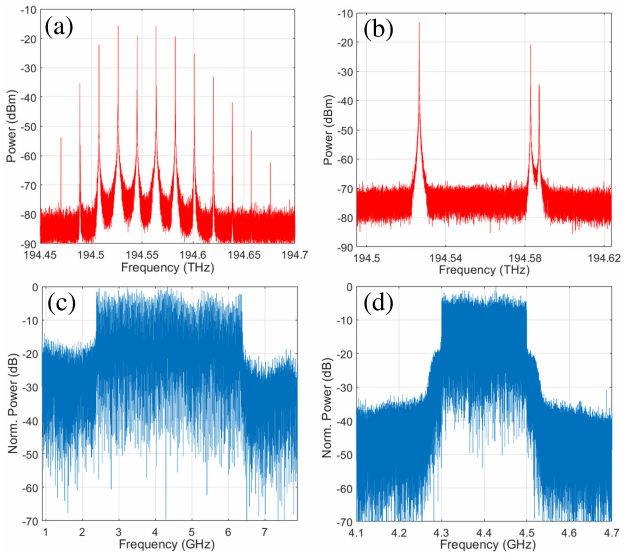

FIGURE 4. Optical spectra; (a) the optical frequency comb source spectrum, (b) the combined SSB modulated and unmodulated carriers launched into the fiber and (c) and (d) the captured electrical IF spectra of the wideband and 5G NR RoF data signals, respectively.

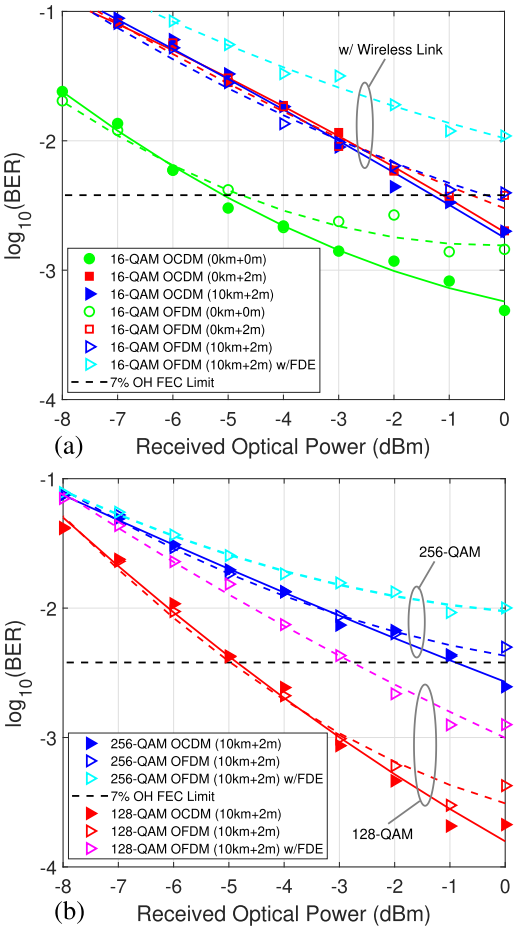

FIGURE 5. Received optical power versus BER for (a) the wideband 16-QAM signal and (b) the mobile 128/256-QAM signals for various transmission cases.

found in [28]). All signals are digitally I/Q up-converted to the IF before being loaded into the AWG. Two sets of OFDM/OCDM multi-carrier numerologies are utilized in this work and are shown in Table 2. The first constitutes a 4 GHz wideband signal delivering 16 Gb/s which could be suitable for future high throughput broadband mm-wave wireless communications. The second set is roughly in line with 5G NR numerology specifications, exhibiting a mobile signal bandwidth of 200 MHz. This signal is modulated using both 128 and 256-QAM resulting in data rates of 1.4 and 1.6 Gb/s, respectively. Figs. 4(c) and (d) show example IF spectra of the captured wideband and mobile signals, respectively.

V. RESULTS AND DISCUSSION

Fig. 5(a) shows the system performance in terms of BER as the received optical power (ROP) is varied. The figure shows results for three transmission scenarios: (i) 0 km + 0 m; back-to-back, (ii) 0 km + 2 m; optical back-to-back with wireless transmission and (iii) 10 km + 2 m; optical and wireless transmission. Fig. 5(a) shows the performance of the wideband OCDM (solid lines) and OFDM (dashed lines) signals. As the ROP is varied, all other system and OCDM/OFDM signal parameters are maintained, including the application of PC+NRW based channel estimation. In the case of OFDM, performance is also evaluated where standard FDE is used (cyan dashed line). Observing the back-to-back performance curves (green) in Fig. 5(a), an error floor emerges for the OFDM signal at ROPs > -4 dBm. This error floor is alleviated by the use of OCDM under the same conditions with BERs of $\leq 1 \times 10^{-3}$ achieved for ROPs > -2 dBm. This performance improvement is a direct result of OCDM's spread spectrum-like features which help to mitigate the effects of the frequency selective mm-wave channel. In this back-to-back scenario, frequency selectivity is caused by the frequency response of the mm-wave components (amplifier, waveguides and mixer) over the relatively large 4 GHz signal bandwidth between 58.5 GHz and 62.5 GHz. At lower ROPs, the two performance curves converge as PD thermal noise becomes the limiting noise process in the system.

Observing the transmission scenarios which include the wireless link in Fig. 5(a), it is clear that the performance improvement which can be achieved by switching to OCDM is reduced compared to the back-to-back case. This is because

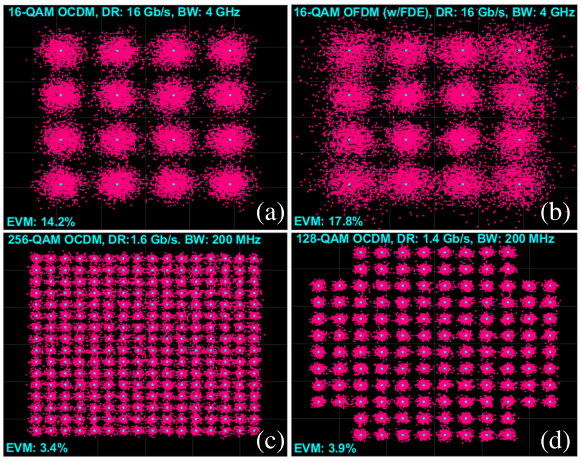

FIGURE 6. Selection of constellation signals received over the full optical and wireless transmission link with a ROP of 0 dBm; (a) wideband 16-QAM OCDM, (b) wideband 16-QAM OFDM with FDE, (c) mobile 256-QAM OCDM and (d) mobile 128-QAM OCDM.

the addition of the wireless link (i.e. one additional V-band amplifier and the horn antennae spaced by 2 m) causes a reduction in electrical signal-to-noise ratio (SNR) resulting in similar performances between OCDM and OFDM up to ROPs of −2 dBm. At higher ROPs, the performance curves (blue and red) diverge as the signal power (and hence SNR) is increased and frequency selectivity once again becomes the performance limiting factor for OFDM signals. The use of OCDM here results in a 1 dB improvement in receiver sensitivity close to the 7% overhead (OH) FEC limit of 3.8×10^{-3}, and BERs below the FEC limit for ROPs of −1 and 0 dBm. It should be noted that the point-to-point wireless transmission path implemented here did not result in significant additional frequency fading or selectivity (which, in this experiment, arise primarily from the mm-wave components used). These results also show that there is a negligible difference in performance between fiber transmission and optical back-to-back cases. This indicates that the effects of fiber dispersion, both on the data signal and on the relative path length difference experienced by the correlated optical carriers, is effectively compensated in the system. In the OFDM transmission case over the full link (cyan dashed line) where standard FDE is employed, the performance is significantly degraded with the emergence of an error floor above the FEC limit at higher ROPs. This highlights the ability of the PC+NRW CE approach to outperform FDE in the presence of Gaussian noise [28]. Figs. 6(a) and (b) show example constellations captured after full link transmission with a ROP of 0 dBm for OCDM (with PC+NRW CE) and OFDM (with FDE), respectively.

Fig. 5(b) shows full link transmission cases for both the OCDM (solid lines) and OFDM (dashed lines) mobile signals with similar trends to the wideband transmission performance results in Fig. 5(a) exhibited. The 256-QAM OFDM signal with FDE exhibits an error floor of 1×10^{-2}. Using PC+NRW CE with this OFDM signal (blue dashed line)

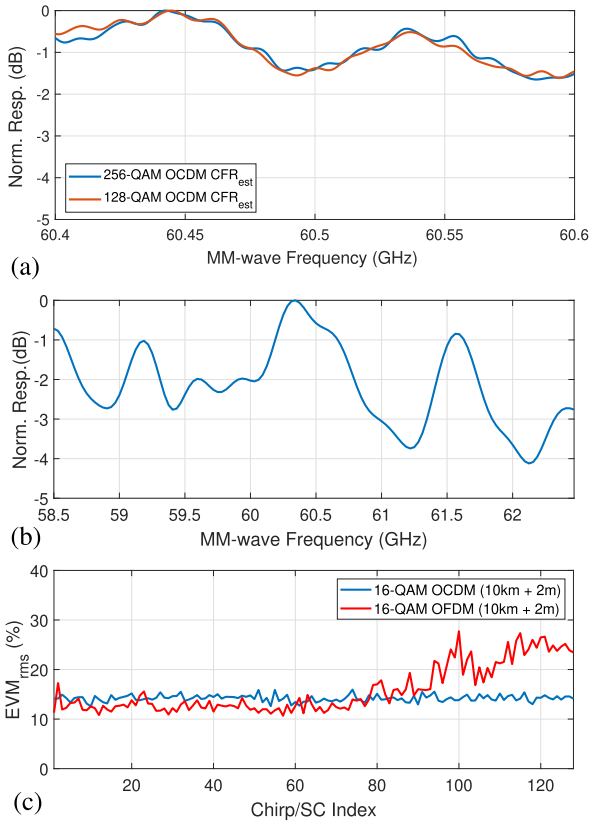

FIGURE 7. Estimated channel frequency response using PC+NRW with (a) narrow-band (200 MHz) signals and (b) the wideband (4 GHz) signal. (c) Shows the received OCDM/OFDM EVM per chirp/subcarrier for the 10 km + 2 m transmission case.

helps to improve performance in this full link transmission scenario, however performance below the FEC limit cannot be achieved. Incorporating enhanced robustness through the transmission of the 256-QAM OCDM signal (solid blue line) results in a further performance improvement with a BER below the FEC limit of 2.46×10^{-3} achieved for a ROP of 0 dBm. As expected, reducing the QAM order to 128 levels results in improved BERs, with all curves exhibiting performances well below the FEC limit at higher ROPs. The 128-QAM OCDM mobile signal (solid red line) provides enhanced performance over the equivalent OFDM signal (dashed red line) with a lowest BER of 2.12×10^{-4} achieved. Again, the transmission of OFDM with FDE (pink dashed line) results in a major degradation in performance with a 3 dB penalty in receiver sensitivity evident at a BER of 1×10^{-3}. Figs. 6(c) and (d) shows the 256 and 128-QAM constellations of the 200 MHz OCDM mobile signals received after transmission over the full link (ROP = 0 dBm) with EVMs of 3.4% and 3.9%, respectively.

Figs. 7(a) and (b) show the mm-wave CFR of the end-to-end optical/mm-wave link estimated through the PC+NRW approach with the narrow-band (128/256-QAM) and wideband (16-QAM) signals, respectively. Fig. 7(c) shows the performance, in terms of EVM per chirp/subcarrier index, of the wideband OCDM/OFDM signals over the full link

with a ROP of 0 dBm. Fig. 7(a) exhibits a relatively flat response with a < 2 dB variation over the 200 MHz channel bandwidth at 60.5 GHz. Moving to the wideband case, the estimated CFR in Fig. 7(b) exhibits a > 4 dB excursion over the 4 GHz mm-wave bandwidth between 58.5 and 62.5 GHz, with the relative severity of frequency selectivity increased above 60.5 GHz. This degraded CFR at higher frequencies is reflected in the EVM versus subcarrier index curve of the OFDM signal in Fig. 7(c) which displays a rise in EVM, up to 27%, for subcarrier indices greater than 70. While the average EVM values of the received OCDM and OFDM signals are similar in this scenario (14.2% and 15.8%, respectively), 7(c) shows that OCDM exhibits a near uniform performance across the entire 4 GHz signal bandwidth. This once again highlights the robustness of the waveform to frequency selectivity, which is attributed to its spread-spectrum features. Such uniformity in performance across the band is highly advantageous for future ultra-high throughput and multi-user access mm-wave communications. While it is possible to achieve a greater uniformity in performance across an OFDM signal bandwidth through the use of power and bit loading of frequency subcarriers, such operation requires CSI to be available at the transmitter through an appropriate feedback link and therefore incurs the additional overhead and processing time associated with closed-loop operation.

While the results described here clearly show how the deployment of OCDM leads to improved performance, the addition of more complex wireless transmission through the use of channel bonding, multiple input multiple output (MIMO) and beamforming would present a more challenging mm-wave environments for which the clear advantages of OCDM could be exploited even further.

VI. CONCLUSION

In conclusion, OCDM has been proposed as a novel waveform in an A-RoF optical/mm-wave C-RAN architecture enabling wireless connectivity for both future wireless broadband and mobile applications. Both a wideband and mobile type OCDM signal have been evaluated in an experimentally constructed end-to-end optical/mm-wave fronthaul test-bed; with OCDM offering improved performance over OFDM in terms of both overall BER and in the uniformity of measured EVM exhibited across a mm-wave bandwidth up to 4 GHz. The use of OCDM here enables performances below the FEC limit to be achieved for all transmission scenarios including full optical and wireless link transmission of a 4 GHz bandwidth 16 Gb/s 16-QAM signal and 200 MHz 1.4/1.6 Gb/s 128/256 signals. The use of a chirped pilot signal inherent to OCDM — facilitating PC-based CE — is shown to significantly improve overall performances compared to the case where OFDM is used in combination with FDE.

Overall, the experimental results presented in this work highlight how emerging photonic and waveform technologies can be combined in a C-RAN architecture to deliver high speed mm-wave services. The use of an A-RoF fronthaul approach here serves to further simplify the RU design making the proposed system more conducive to wide network deployment. The optical heterodyne technique employed can offer flexibility in remote carrier generation frequency and is enabled through a centralized transmitter design which, through photonic integration, could potentially be incorporated into a full transceiver. The unique combination of these aspects, coupled with OCDM's robustness and compatibility with standard OFDM signal processing procedures, can lead the way to the development of flexible converged access systems capable of delivering high-speed broadband and mobile services in challenging mm-wave and even THz environments.

ACKNOWLEDGMENT

The authors would like to acknowledge Amol Delmade for his valuable discussions regarding the experimental work.

REFERENCES

[1] M. Z. Chowdhury, M. Shahjalal, S. Ahmed, and Y. M. Jang, "6G wireless communication systems: Applications, requirements, technologies, challenges, and research directions," *IEEE Open J. Commun. Soc.*, vol. 1, pp. 957–975, 2020.

[2] H. Tataria, M. Shafi, A. F. Molisch, M. Dohler, H. Sjöland, and F. Tufvesson, "6G wireless systems: Vision, requirements, challenges, insights, and opportunities," 2020, *arXiv:2008.03213*.

[3] B. Zong, C. Fan, X. Wang, X. Duan, B. Wang, and J. Wang, "6G technologies: Key drivers, core requirements, system architectures, and enabling technologies," *IEEE Veh. Technol. Mag.*, vol. 14, no. 3, pp. 18–27, Sep. 2019.

[4] A. S. Cacciapuoti, K. Sankhe, M. Caleffi, and K. R. Chowdhury, "Beyond 5G: THz-based medium access protocol for mobile heterogeneous networks," *IEEE Commun. Mag.*, vol. 56, no. 6, pp. 110–115, Jun. 2018.

[5] *Enhanced Throughput for Operation in License-Exempt Bands Above 45 GHz*, Standard 802.11ay-2021, Jul. 2021.

[6] F. Saliou, P. Chanclou, L. A. Neto, G. Simon, J. Potet, M. Gay, L. Bramerie, and H. Debregeas, "Optical access network interfaces for 5G and beyond [invited]," *J. Opt. Commun. Netw.*, vol. 13, no. 8, p. D32, Aug. 2021.

[7] K. Bourg, S. Ten, R. Whitman, J. Jensen, and V. Diaz, "The evolution of outside plant architectures driven by network convergence and new PON technologies," in *Proc. Opt. Fiber Commun. Conf.*, Mar. 2017, pp. 1–3.

[8] C. Browning, Q. Cheng, N. C. Abrams, M. Ruffini, L. Y. Dai, L. P. Barry, and K. Bergman, "A silicon photonic switching platform for flexible converged centralized-radio access networking," *J. Lightw. Technol.*, vol. 38, no. 19, pp. 5386–5392, Oct. 1, 2020.

[9] *Radio-Over-Fibre (RoF) Technologies and Their Applications*, document ITU-T, Series G Supplement 55, 2015, pp. 29–33.

[10] P. Perry, C. Browning, B. Scotney, A. Delmade, S. McClean, L. Barry, A. Peters, and P. Morrow, "Comparison of analogue and digital fronthaul for 5G MIMO signals," in *Proc. IEEE Int. Conf. Commun. (ICC)*, Jun. 2020, pp. 1–6.

[11] C. Browning, H. H. Elwan, E. P. Martin, S. O'Duill, J. Poette, P. Sheridan, A. Farhang, B. Cabon, and L. P. Barry, "Gain-switched optical frequency combs for future mobile radio-over-fiber millimeter-wave systems," *J. Lightw. Technol.*, vol. 36, no. 19, pp. 4602–4610, Oct. 1, 2018.

[12] C. Browning, A. Delmade, Y. Lin, J. Poette, H. H. Elwan, and L. P. Barry, "Phase noise robust optical heterodyne system for reduced complexity millimeter-wave analog radio-over-fibre," in *Proc. 45th Eur. Conf. Opt. Commun. (ECOC)*, Sep. 2019, pp. 1–4.

[13] A. Delmade, C. Browning, T. Verolet, J. Poette, A. Farhang, H. H. Elwan, R. D. Koilpillai, G. Aubin, F. Lelarge, A. Ramdane, D. Venkitesh, and L. P. Barry, "Optical heterodyne analog radio-over-fiber link for millimeter-wave wireless systems," *J. Lightw. Technol.*, vol. 39, no. 2, pp. 465–474, Jan. 15, 2021.

[14] C. Browning, X. Ouyang, D. Dass, G. Talli, and P. Townsend, "Orthogonal chirp-division multiplexing for performance enhanced optical/millimeter-wave 5G/6G communications," in *Proc. Opt. Fiber Commun. Conf. (OFC)*, Jun. 2021, pp. 1–3.

[15] X. Ouyang and J. Zhao, "Orthogonal chirp division multiplexing," *IEEE Trans. Commun.*, vol. 64, no. 4, pp. 3946–3957, Sep. 2016.
[16] X. Ouyang, O. A. Dobre, Y. L. Guan, and J. Zhao, "Chirp spread spectrum toward the Nyquist signaling rate—Orthogonality condition and applications," *IEEE Signal Process. Lett.*, vol. 24, no. 10, pp. 1488–1492, Oct. 2017.
[17] F. Lu, L. Cheng, M. Xu, J. Wang, S. Shen, and G.-K. Chang, "Orthogonal chirp division multiplexing in millimeter-wave fiber-wireless integrated systems for enhanced mobile broadband and ultra-reliable communications," in *Proc. Opt. Fiber Commun. Conf.*, Mar. 2017, pp. 1–3.
[18] P. T. Dat, Y. Yamaguchi, A. Kanno, M. Motoya, S. Oikawa, J. Ichikawa, and N. Yamamoto, "Millimeter-wave radio-over-fiber system using optical phase modulation and photonic downconversion for uplink fronthaul transmission," *Opt. Lett.*, vol. 46, pp. 2493–2496, 2021.
[19] M. Sung, J. Kim, E.-S. Kim, S.-H. Cho, Y.-J. Won, B.-C. Lim, S.-Y. Pyun, H. Lee, J. K. Lee, and J. H. Lee, "RoF-based radio access network for 5G mobile communication systems in 28 GHz millimeter-wave," *J. Lightw. Technol.*, vol. 38, no. 2, pp. 409–420, Jan. 15, 2020.
[20] N. Argyris, G. Giannoulis, K. Kanta, N. Iliadis, C. Vagionas, S. Papaioannou, G. Kalfas, D. Apostolopoulos, C. Caillaud, H. Debregeas, N. Pleros, and H. Avramopoulos, "A 5G mmWave fiber-wireless IFoF analog mobile fronthaul link with up to 24-Gb/s multiband wireless capacity," *J. Lightw. Technol.*, vol. 37, no. 12, pp. 2883–2891, Jun. 15, 2019.
[21] A. Val Marti, N. Vokic, M. Hofer, D. Milovancev, T. Zemen, and B. Schrenk, "Hybrid analogue/digitized radio-over-fibre downlink through orthogonal optical mm-wave and 10 Gb/s baseband transport," in *Proc. Eur. Conf. Opt. Commun. (ECOC)*, Sep. 2021, pp. 1–4.
[22] K. Kasai, T. Sato, T. Hirooka, M. Yoshida, and M. Nakazawa, "64 Gbit/s, 256 QAM transmission through coherent optical-wireless link at 61 GHz using simple and high OSNR carrier frequency converter," in *Proc. Opt. Fiber Commun. Conf. (OFC)*, Jun. 2021, pp. 1–3.
[23] S. E. Alavi, M. R. K. Soltanian, I. S. Amiri, M. Khalily, A. S. M. Supa'at, and H. Ahmad, "Towards 5G: A photonic based millimeter wave signal generation for applying in 5G access fronthaul," *Sci. Rep.*, vol. 6, no. 1, Jan. 2016, Art. no. 19891.
[24] D. Konstantinou, A. Morales, S. Rommel, T. R. Raddo, U. Johannsen, and I. T. Monroy, "Analog radio over fiber fronthaul for high bandwidth 5G millimeter-wave carrier aggregated OFDM," in *Proc. 21st Int. Conf. Transparent Opt. Netw. (ICTON)*, Jul. 2019, pp. 1–4.
[25] Y. Tong, C.-W. Chow, G.-H. Chen, C.-W. Peng, C.-H. Yeh, and H. K. Tsang, "Integrated silicon photonics remote radio frontend (RRF) for single-sideband (SSB) millimeter-wave radio-over-fiber (ROF) systems," *IEEE Photon. J.*, vol. 11, no. 2, pp. 1–8, Apr. 2019.
[26] Y. Tian, K.-L. Lee, C. Lim, and A. Nirmalathas, "Demonstration of non-orthogonal multiple access scheme using multilevel coding without successive interference cancellation with 60 GHz radio-over-fiber fronthaul," in *Proc. Opt. Fiber Commun. Conf.*, Mar. 2018, pp. 1–3.
[27] A. Delmade, T. Verolet, C. Browning, Y. Lin, G. Aubin, F. Lelarge, A. Ramdane, and L. P. Barry, "Quantum dash passively mode locked laser for optical heterodyne millimeter-wave analog radio-over-fiber fronthaul systems," in *Proc. Opt. Fiber Commun. Conf. (OFC)*, Mar. 2020, pp. 1–3.
[28] X. Ouyang, C. Antony, G. Talli, and P. D. Townsend, "Robust channel estimation for coherent optical orthogonal chirp-division multiplexing with pulse compression and noise rejection," *J. Lightw. Technol.*, vol. 36, no. 23, pp. 5600–5610, Dec. 1, 2018.

COLM BROWNING (Member, IEEE) received the Honours degree in electronic engineering (BAI) and a minor in mathematics (BA) from the Trinity College Dublin, in 2009, and the Ph.D. degree in reconfigurable optical systems from Dublin City University (DCU), Ireland, in 2013. He is a Senior Research Fellow at the School of Electronic Engineering, DCU, where he is currently leading a research at the Radio and Optical Communications Laboratory, focusing on converged optical systems for next-generation datacenter, access, and mobile networks.

DEVIKA DASS (Student Member, IEEE) received the Bachelor of Technology degree in electronics and telecommunication from Amity University, India, in 2014, and the master's degree in communication engineering from VIT University, Vellore, India, in 2015. She is currently pursuing the Ph.D. degree with the Radio and Optical Communications Laboratory, Dublin City University. In 2017, she joined IIT Delhi as a Research Fellow. Her current research interests include advanced modulation formats and their applications in converged optical access networks, millimeter-wave generation, characterization, and applications of tunable semiconductor lasers, coherent optical communications, and free space optical communications.

PAUL TOWNSEND (Member, IEEE) received the Ph.D. degree in physics from the University of Cambridge, in 1987. He subsequently worked with the international communications industry at Bell Communications Research, BT, and Corning, where he held research leadership positions, before moving to the Tyndall National Institute, Cork, Ireland, in 2003. He is also an Honorary Professor with the School of Engineering and Physical Sciences, Heriot-Watt University, Edinburgh, and a fellow of the Institute of Physics. He has authored more than 170 peer-reviewed publications, including 40 invited papers, and holds granted patents in 16 families to date, with several other applications pending.

XING OUYANG (Member, IEEE) received the Ph.D. degree from University College Cork, Ireland, in 2017. He is currently with the Tyndall National Institute, University College Cork. His current research interests include the multicarrier transmission techniques and digital signal processing in high-speed wireless and optical communication systems.